Referenceless Reconstruction in Simultaneous Multi-Slice Imaging

Klaus Eickel,[1,2*] Matthias Günther,[1,2]

[1] Fraunhofer MEVIS, Bremen, Deutschland.
[2] mediri GmbH, Heidelberg, Deutschland.
* klaus.eickel@mevis.fraunhofer.de

Abstract: The unwrapping of simultaneous multi-slice images without extra reference data is presented. A trained deep neural network disentangles overlapping image content and creates the final magnitude image. The results are compared to established techniques when correct reference are missing.

Zusammenfassung: Es wird die Entfaltung von überlagerten Bildinhalten bei der gleichzeitigen Mehrschichtaufnahme durch ein trainiertes tiefes Neuronales Netz präsentiert, ohne dabei zusätzliche Referenzmessungen zu nutzen. Die Rekonstruktionsergebnisse werden anschließend mit den etablierten Verfahren verglichen, besonders, wenn auch hier keine geeigneten Referenzdaten verfügbar sind.

Motivation

Simultaneous multi-slice (SMS) imaging (1–3) has emerged as a promising acceleration technique for magnetic resonance imaging (MRI) since multi-coil systems (4) and reconstruction methods like slice-GRAPPA (5) paved the way for SMS in a variety of applications. The established reconstruction strategies for SMS utilize spatial encoding information inherent in multi-coil receiver arrays. This requires additionally acquired reference data, i.e. auto-calibration signal (ACS), to disentangle spatially overlapping image content (6).
In this work, a deep neural network (DNN) was designed and trained to unfold SMS images without the need of any reference scans. First, the DNN architecture is introduced. Thereafter, the predicted images are evaluated and the Deep Learning (DL) reconstruction (DLR) is compared to split slice-GRAPPA (SSG) (7) reconstructions where correct reference data are missing.

Material and Methods

Training a DNN requires suitable data. 37 datasets of phantom objects (N=30) and heads (N=7) were used for training (N_{train}=29) and validation (N_{val}=8), while evaluation was done on separate datasets of volunteers' heads (N_{test}=4). All data were acquired with identical sequence parameters giving a volume of 128x128x6 px^3 in 3 contrasts (TE=4.9/9.7/14.5 ms). Rawdata of 20 receiver coils were preprocessed offline, e.g. simulated SMS acquisition and CAIPIRINHA-shifts (8), and augmented by undersampling (90%, 80%, 75%, 70%, 60%, 50%, 40%, 30%) yielding to N_{train}=2349, N_{val}=648 datasets for a multiband factor (MB) of MB=2 and N_{train}=870, N_{val}=240 for MB=3, respectively. Figure 1 shows the DNN's architecture where folded (MB=2 or MB=3), uncombined, low-resolution k-space (64x64 px^2) and image data (128x128 px^2) were fed into the network while sum-of-square combined and disentangled magnitude images serve as target. Real and imaginary component of the complex-valued input were concatenated along the channel dimension (N_{ch}=40). A user defined loss-function: $E = MSE \times TV$ was applied to drive the training process, where mean-squared error (*MSE*) and total-variation error (*TV*) were combined to account for global errors as well as mismatches on object borders. The DNN was set up in the Keras library (9) and training (280 epochs, duration about 28 hours) was performed on a Nvidia GTX1080 graphics card.

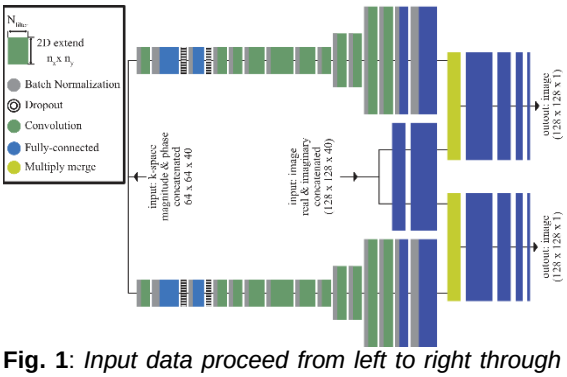

Fig. 1: *Input data proceed from left to right through the different layers. System features similar to coil-sensitivities are derived from the k-space data. These are then merged with the preprocessed image input to unwrap overlapping image content. In the following layers, the channels are combined yielding a single magnitude image per slice, e.g. two unwrapped images for MB=2.*

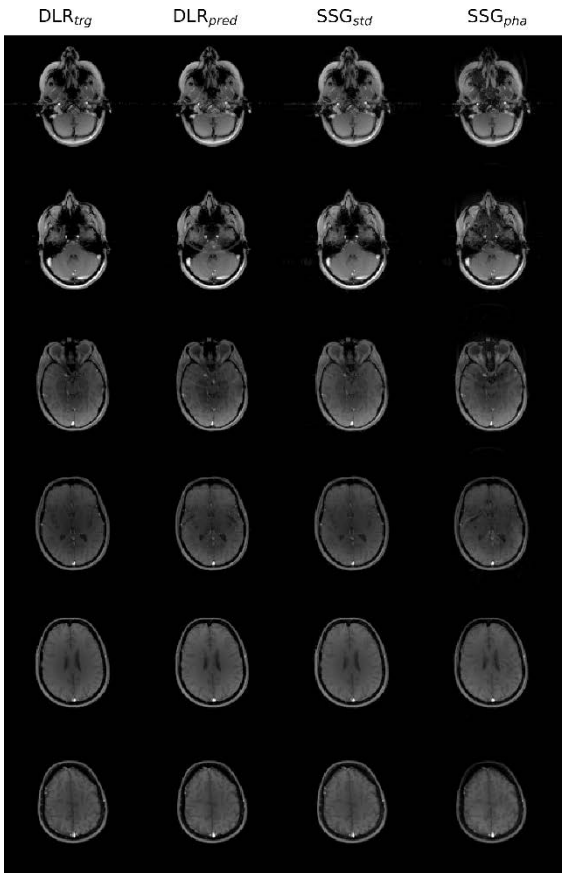

Fig. 2: Comparison of reconstructions for a MB=2 with a CAIPIRIINHA shift of ¼ FOV. The target data (DLR_{trg}) represent the ground truth for the prediction of the DNN (DLR_{pred}) as well as for standard SSG_{std} reconstruction with correct ACS and SSG_{pha} reconstruction with incorrect ACS of a spherical phantom.

Results

Unseen test volumes were fed into the trained DNN and its predictions were evaluated visually and compared to SSG reconstructions with suitable ACS (SSG_{std}) and ACS of a spherical phantom (SSG_{pha}) (Fig. 2). All images I are slice-wise normalized to their minimum and maximum pixel values by $I_{norm}=(I - I_{min})/(I_{max} - I_{min})$ which allows quantitative analysis. Background noise in the SSG images is removed by thresholding (3%).

Normalized subtraction maps (Fig. 3) compare the reconstructions of the presented approach to standard SSG where correct ACS are missing and replaced by ACS of another head (SSG_{01}) and ACS of a spherical phantom (SSG_{pha}). In both cases the FOV was kept in identical position.

Two metrics were derived to quantify the reconstruction performance. The normalized root mean-squared error (NRMSE) and the structural similarity index (SSIM) (10) across the total volume as listed in Tab. 1 suggest that DLR (second column) performs better than SSG with incorrect ACS (last two columns), but leads to more reconstruction errors than SSG where correct ACS are available (first column).

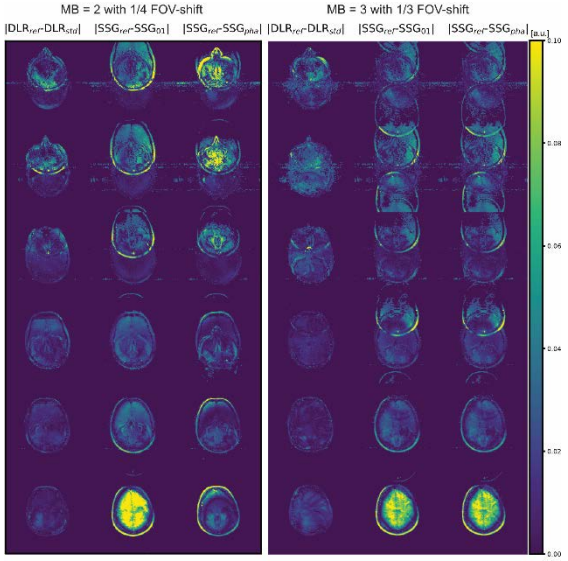

Fig. 3: Normalized subtraction maps of all slices are shown. Reconstruction where no correct ACS are available suffer from various artifacts, e.g. leakage. DLR (left) without any ACS is compared to SSG with ACS of another head dataset (middle) and ACS of a spherical phantom (right).

[x 10^{-2}]	SSG_{std}	DLR	SSG_{01}	SSG_{pha}
NRMSE	3.35	9.17	19.6	16.2
SSIM	99.8	99.2	95.3	96.8
NRMSE	3.59	9.19	17.5	17.4
SSIM	99.8	99.0	94.9	94.6

Tab. 1: *NRMSE and SSIM for the reconstruct-ion of MB=2 datasets are shown in the first and second row (light gray). The last two rows list these metrics for MB=3 (gray).*

Discussion

In this work a novel approach to reconstruct SMS images without the need of additional ACS data is presented. Although, clearly more reconstruction artifacts as for a correct SSG reconstruction occur, DLR is beneficial to SSG with incorrect reference data. This might be especially useful in case of dynamic image in presents of motion. As in other DL scenarios, it is likely that the performance of the presented DNN can be significantly increase when additional training data are included.

References

1. Weaver JB. Simultaneous multislice acquisition of MR images. Magn Reson Med 1988;8:275–284.

2. Müller S. Multifrequency selective rf pulses for multislice MR imaging. Magn Reson Med 1988;6:364–371.

3. Souza SP. Simultaneous Multislice Acquisition of MR Images by Hadamard-Encodes Excitation SOUZA_1988.pdf.

4. Larkman DJ, Hajnal J V., Herlihy AH, Coutts GA, Young IR, Ehnholm G. Use of multicoil arrays for separation of signal from multiple slices simultaneously excited. J Magn Reson Imaging 2001;13:313–317.

5. Setsompop K, Gagoski BA, Polimeni JR, Witzel T, Wedeen VJ, Wald LL. Blipped-controlled aliasing in parallel imaging for simultaneous multislice echo planar imaging with reduced g-factor penalty. Magn Reson Med 2012;67:1210–1224.

6. Barth M, Breuer F, Koopmans PJ, Norris DG, Poser BA. Simultaneous multislice (SMS) imaging techniques. Magn Reson Med 2016;75:63–81.

7. Cauley SF, Polimeni JR, Bhat H, Wald LL, Setsompop K. Interslice leakage artifact reduction technique for simultaneous multislice acquisitions. Magn Reson Med 2014;72:93–102.

8. Breuer FA, Blaimer M, Heidemann RM, Mueller MF, Griswold MA, Jakob PM. Controlled aliasing in parallel imaging results in higher acceleration (CAIPIRINHA) for multi-slice imaging. Magn Reson Med 2005;53:684–691.

9. Chollet F et al. Keras. 2015.

10. Wang Z, Bovik AC, Sheikh HR, Member S, Simoncelli EP, Member S. Image Quality Assessment: From Error Visibility to Structural Similarity. 2004;13:600–612.